Increasing the CO_2 Reduction Activity of Cobalt Phthalocyanine by Modulating the σ-donor Strength of Axially Coordinating Ligands

Kevin E. Rivera Cruz[†,#], *Yingshuo Liu*[†,#], *Taylor L. Soucy, Paul M. Zimmerman**[,†], *and Charles C. L. McCrory**[,†,§]

[†]Department of Chemistry, University of Michigan, Ann Arbor, Michigan, 48109-1055, United States.

[§]Macromolecular Science and Engineering Program, University of Michigan, Ann Arbor, Michigan, 48109-1055, United States.

[#]K.E.R.C. and Y.L. contributed equally.

ABSTRACT

Axial coordination of a pyridyl moieties to CoPc (either exogenous or within poly-4-vinylpyridine polymer) dramatically increases the complex's activity for CO_2RR. It has been hypothesized that axial coordination to the Co active site leads to an increase in the Co dz^2 orbital energy, which increases the complex's nucleophilicity and facilitates CO_2 coordination compared to the parent CoPc complex. The magnitude of the energy increase in the Co dz^2 orbital should depend on the σ-donor strength of the axial ligand—a stronger σ-donating ligand (L) will increase the overall CO_2RR activity of axially coordinated CoPc(L) and vice versa. To test this, we have studied a series of CoPc(L) complexes where the σ-donor strength of L is varied. We show that CoPc(L) reduces CO_2 with an increased activity as the σ-donor ability of L is increased. These observed electrochemical activity trends are correlated with

computationally-derived CO_2 binding energy and charge transfer terms as a function of σ-donor strength. The findings of this study supports our hypothesis that the increased CO_2RR activity observed upon axial coordination to CoPc is due to the increased energy of the dz^2 orbital, and highlight an important design consideration for macrocyclic MN_4-based electrocatalysts.

INTRODUCTION

The electrochemical conversion of CO_2 into energy-rich fuels and chemicals in the CO_2 reduction reaction (CO_2RR) has gained significant interest as a promising strategy for effectively storing intermittent renewable energy from sources such as solar and wind.[1-14] There is an increasing drive to discover new catalysts that reduce CO_2 into value-added products or chemical feedstocks, including CO,[12-14] with high activity and selectivity at low overpotentials. Physically-motiviated design principles help guide the rational design of new CO_2RR catalyst systems, and these design principles can be tested and verified by evaluation of how systematic modifications of catalyst model systems influence electrocatalytic activity and selectivity. Surface-immobilized cobalt phthalocyanine (CoPc) is a model system of particular interest to the electrocatalysis community; it was first reported as an active catalyst for the CO_2RR over 35 years ago,[15,16] and since then its catalytic activity has been extensively explored under various aqueous conditions.[17-42]

Our group's interest in CoPc lay in its utility as a model system for studying the effects of polymer encapsulation on electrocatalytic performance. In particular, we are interested in probing how changing a catalyst's coordination environment due to polymer encapsulation influences its electrocatalytic activity and selectivity for multielectron small-molecule transformations such as the CO_2RR.[43] Physisorbed CoPc on carbon electrodes with no polymer binder shows only modest activity for the CO_2RR in aqueous phosphate and citrate solutions with appreciable H_2 generated from the competitive hydrogen evolution

reaction (HER).[15,17,18,21,22] Work by our group[17,19] and others[21,22] has shown that encapsulating CoPc within coordinating polymers like poly-4-vinylpyridine (P4VP) results in CoPc-P4VP composite materials that operate with increased activity and selectivity for the electrochemical reduction of CO_2 to CO compared to the parent physisorbed CoPc complexes. This increase in activity and selectivity has been attributed to three distinct effects of the polymer on the coordination environment of the Co active site in CoPc-P4VP: i) axial-coordination of pyridyl in P4VP to the Co center increases the catalyst's nucleophilicity for CO_2 binding, ii) H-bonding interactions that stabilize reactive CO_2 intermediates, and iii) control of H^+ delivery through a multi-site proton relay mechanism involving the polymer's pyridyl residues (Figure 1).[17,18,22] Axial coordination plays an important role in modulating the activity[17,18,23,29] and mechanism[18,19] of the CO_2RR by CoPc systems. For instance, we have previously shown that upon axial coordination of pyridine = L3 to CoPc to form the CoPc(L3) complex, there is a change in the rate-determining step of the mechanism from an initial CO_2 coordination step for CoPc to a subsequent protonation event for CoPc(L3).[18]

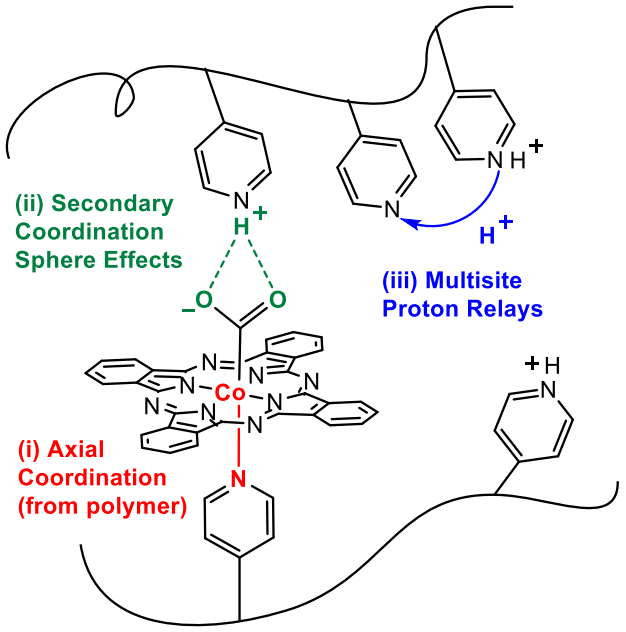

Figure 1. Illustration of CoPc-P4VP highlighting the i) axial-coordination to the pyridyl residues from the P4VP polymer in the primary coordination sphere, ii) the H-bonding stabilization of reduced CO_2 intermediates in the secondary coordination sphere, and iii) the controlled H^+ delivery via a multisite proton relay in the outer coordination sphere. Adapted from Ref. 19 with permission from The Royal Society of Chemistry.

Based on the studies described above, we hypothesize that axial coordination of σ-donating ligands (L) to CoPc increases the nucleophilicity of the Co center in the CoPc(L) complexes by increasing the energy of the dz^2 orbitals. This, in turn, increases the ability of the Co center to coordinate and activate the Lewis acidic carbon of CO_2. Based on this hypothesis, we expect that increasing the σ-donating ability of the axial ligand on CoPc(L) should further increase the relative energy of the dz^2 orbital resulting in higher activity for the CO_2RR. In this report, we test this hypothesis by conducting a combined electrochemical and computational study on CoPc(L) complexes with various axial ligands (L). A list of the axial ligands used in this study are shown in Figure 2 in order of increasing σ-donor strength from

lowest (L1) to highest (L8) as indicated by the reported coupling constant between the donor group and the methylmercury (II) cation.[44-48] We demonstrate that as the σ-donor strength of the axial ligand increases, there is a corresponding increase in the catalytic activity of the CoPc(L) for the CO_2RR. Using density functional theory analysis, we show that axial coordination does, in fact, increase the energy of the dz^2 orbital, and that the experimentally-observed increase in CO_2RR activity with increasing σ-donor strength of the axial ligand is correlated to an increased extent of charge transfer from the reduced CoPc(L) complex to CO_2 adduct. Overall, our work highlights the role of axial coordination in modulating activity for the CO_2RR and provides important insights into the design of highly active CoPc-based systems for selective CO_2 conversion.

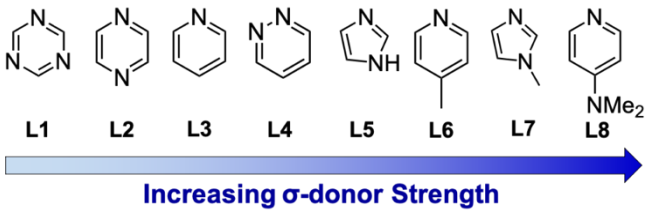

Figure 2. Axially-coordinating ligands (L) investigated in this study, listed in order of increasing σ-donor strength from lowest (L1) to highest (L8). L1 = 1,3,5-triazine, L2 = pyrazine, L3 = pyridine, L4 = pyridazine, L5 = imidazole, L6 = 4-methylpyridine, L7 = 1-methyl imidazole, and L8 = 4-dimethylaminopyridine.

EXPERIMENTAL

Materials and Supplies

All purchased chemicals were used as received unless otherwise specified. Cobalt phthalocyanine (CoPc, 97%), N,N-dimethylformamide (DMF, ACS grade), 1,3,5-triazine (L1, 97%), pyrazine (L2, >99%), pyridine (L3, ACS grade, ≥ 99%), pyridazine (L4, 98%), imidazole (L5, 99%), 4-methyl pyridine

(L6, 99%), 1-methyl imidazole (L7, ≥ 99%), 4-dimethylaminopyridine (L8, ≥ 99%), sodium phosphate monobasic (BioXtra, > 99.0%), ferrocenecarboxylic acid (97%), and sodium hydroxide (NaOH, BioXtra, ≥ 98% were purchased from Sigma Aldrich. Nitric acid (HNO_3, TraceMetal grade, 67-70%) was purchased from Fisher Scientific. Nafion-117 cation exchange membranes (Nafion) were purchased from the Fuel Cell Store. Nitrogen (N_2) was boil-off gas from a liquid nitrogen source. Compressed CO_2 gas (99.8%) was purchased from Cryogenic Gases. All water used in this study was ultrapure water (18.2 MΩ·cm resistivity) purified with a Thermo Scientific GenPure UV-TOC/UF xCAD-plus water purification system.

Preparation of CoPc(L)-modified Edge Plane Graphite Electrodes

Deposition solutions for CoPc and CoPc(L) were prepared based on an adaptation of previously described procedure.[18] 0.05 mM CoPc/DMF deposition solutions were prepared by dissolving 0.13 mg of CoPc in 45 mL DMF and sonicating for at least 30 min until the CoPc was fully dispersed. To prepare CoPc(L)/DMF deposition solutions, 2.25 mmol of the axial ligand L was added to 45 mL of the 0.05 mM CoPc/DMF deposition solution, and the resulting solution was sonicated for at least 30 min until the CoPc and L were fully dispersed. Note that for the liquid ligands CoPc(L3), CoPc(L4), CoPc(L6) and CoPc(L7) in DMF deposition solution, the CoPc and Ligands were dissolved with 10mL of DMF, it was vortexed for 1 min and sonicated for 10 min prior the addition of the remainding 35mL DMF to favor the complex formation. For the solid ligands CoPc(L1), CoPc(L2), CoPc(L5) and CoPc(L8) in DMF deposition solutions, ~60 min of sonication time was used to ensure full dispersion of CoPc and L. The final concentrations in the CoPc(L)/DMF deposition solutions was 0.05 mM CoPc and 50 mM L. The large excess of the axial ligand (~1,000×) used in the deposition solutions was to ensure equilibrium favored the axially-coordinated species.[49]

Prior to deposition, 5 mm diameter edge plane graphite (EPG) disk electrodes (3.81 mm EPG disk encapsulated in epoxy, 0.114 cm^2 effective surface area, Pine Research Instrumentation) were manually polished with 600 grit SiC grinding paper (Buehler CarbiMet) followed by sonication in ultrapure water for ~ 1 min. The CoPc- and CoPc(L)-modified CoPc EPG working electrodes were then prepared by dropcasting 5 μL of the CoPc/DMF deposition solution or the CoPc(L)/DMF deposition solution onto the EPG electrode. The disk electrodes were then placed in a drying oven at ~60-70 °C for ~15 min to allow the solvent to evaporate. The resulting loading of CoPc or CoPc(L) on the electrode surface is calculated as 2.19×10^{-9} mol cm^{-2}.

Electrochemical Measurements

Electrochemical measurements were conducted using a Bio-Logic SP200 potentiostat, and data were recorded using the Bio-Logic EC-Lab software package. Reference electrodes were commercial saturated calomel electrodes (SCE, CH Instruments) externally referenced to ferrocenecarboxylic acid in 0.2 M phosphate buffer at pH 7 (0.284 V vs. SCE),[50] and auxiliary electrodes were carbon rods (99.999 %, Strem Chemicals Inc.). Unless otherwise noted, all electrochemical measurements were conducted at least three times with independently prepared electrodes, and reported values are the averages of these repetitions with standard deviations included as the reported errors. The electrolyte solution used for all electrochemical studies was a pH 5 phosphate solution prepared from a 0.1 M NaH_2PO_4 solution adjusted to pH 5 by the addition of aqueous 1 M NaOH. The solution pH was confirmed using a Fisher Scientific Accumet AB200 pH meter with an Accumet pH/ATC Epoxy Body Combination Electrode calibrated with a 3-point calibration curve at pH = 4.01, 7.00, and 10.01.

Rotating Disk Electrode Voltammetry and Chronoamperometry Experiments. For rotating disk electrode voltammetry (RDEV) experiments and rotating disk electrode chronoamperometric step (RDE-

CA) measurements, the working electrodes were mounted into a Pine Research Instrumentation E6-series Change Disk rotating disk electrode (RDE) assembly attached to an MSR rotator. RDEV and RDE-CA measurements were conducted at room temperature in a custom two-compartment glass H-cell as previously described.[18] The working and reference electrodes were submerged in ~30 mL solution in the first compartment, and the auxiliary electrode was submerged in ~15 mL solution in the second compartment. The two compartments were separated by a Nafion cation exchange membrane. Both compartments were sparged with CO_2 for ~30 min prior to each set of measurements, and the headspace was blanketed with CO_2 during the measurements. The CO_2 used was first saturated with electrolyte solution by bubbling through a gas washing bottle filled with the same electrolyte solution used in the cell to minimize electrolyte evaporation in the cell during the measurements. RDEV measurements were measured at 1600 rpm rotation rate and a scan rate of 1 mV s^{-1}. RDE-CA measurements were conducted at 1600 rpm with 2-min potential steps from -0.95 V to -1.35 V vs. SCE at 0.05 V increments. The 1600 rpm rotation rate was meant to ensure steady-state delivery of substrate to our surface to allow for accurate comparisons of catalytic rates. Note that 1600 rpm does not imply kinetically-limiting conditions—mass transport to catalyst sites in non-uniform catalyst-polymer composite films is not governed by simple Koutecký-Levich kinetics.[51-54] The uncompensated resistance of the cell (R_u) was measured with a single-point high-frequency impedance measurement, and RDEV and RDE-CA measurements were corrected for IR-drop at 85% through positive feedback using the Bio-Logic EC-Lab software. In general, our electrochemical cell for RDEV and RDE-CA measurements had $R_u \approx 100\ \Omega$ when filled with our pH 5 phosphate electrolyte solution.

Controlled Potential Electrolysis Experiments. Controlled potential electrolyses (CPE) were conducted at room temperature in a custom, gas-tight two compartment U-cell as previously described.[18] The working electrode was held in a RDE internal hardware kit (Pine Research Instrumentation) and

mounted into a custom-designed PEEK sleeve. The first compartment of the U-cell held the working electrode and reference electrode in 25 mL of electrolyte, and the second compartment held the auxiliary electrode in ~15 mL electrolyte. The two compartments were separated by a Nafion cation exchange membrane. The total volume of the first chamber was measured after each experiment by measuring the volume of H_2O necessary to completely fill the chamber when the cell was fully assembled with the working and reference electrodes, and the headspace volume for the CPE measurements was calculated by subtracting the electrolyte volume of 25 mL from the total volume of the first chamber. Prior to each experiment, both chambers were sparged with CO_2 for ~ 30 min and then the main chamber was sealed under CO_2 atmosphere. The uncompensated resistance of the cell was measured with a single-point high-frequency impedance measurement. In general, our electrochemical cell for CPE had R_u = ~200 Ω in pH 5 phosphate solution. The CPE measurements were conducted with no iR compensation, and the reported electrolysis potentials are the actual applied potentials.

Product detection and quantification were conducted as previously described.[18] CO and H_2 were detected on a Thermo Scientific Trace 1310 Gas Chromotography system with two analyzer channels for the detection of H_2 and C1-C2 products. After each electrolysis, a 5 mL aliquot of the headspace in the first compartment of the cell was collected using a Pressure-Lok gastight syringe (10 mL, Valco VICI Precision Sampling, Inc.), and the aliquot was injected into a 3 mL sample loop on the gas chromatograph. Using a custom valve system, column configuration, and method provided by Thermo Scientific, gases were separated such that H_2 was detected on the first channel using an Ar carrier gas and thermal conductivity detector (TCD), and all other gases were detected on the second channel using a He carrier gas and a TCD. The GC system was calibrated using calibration gas mixtures (SCOTTY Specialty Gas) at H_2 = 0.02, 0.05, 0.5, and 1% v/v, and CO = 0.02, 0.05, 0.5, 1, and 7% v/v. Chromatographs were analyzed using the Chromeleon Console Workstation software. To determine the concentration of

dissolved products in the electrolyte solution, 1 mL aliquots of the post-electrolysis solutions were analyzed using a Thermo Scientific UltiMate 3000 HPLC system equipped with a refractive index detector (RFD), a 5 cm Thermo Scientific™ HyperREZ™ XP Carbohydrate H^+ LC guard column and a 30 cm Thermo Scientific™ HyperREZ™ XP Carbohydrate H^+ LC analytical column in series using a 5 mM H_2SO_4 aqueous mobile phase at a constant temperature of 50 °C. The detection limit of the HPLC for formic acid was determined to be 0.1 mM. No formic acid was observed after the CO_2RR CPEs.

Faradaic Efficiencies (FE) were calculated by dividing the moles of each product detected by the total moles of electrons based on the charge passed during the CPE according to Equation 1:

$$FE = \frac{\frac{V_{\mathrm{HS}}}{V_{\mathrm{m}}} \times C \times nF}{Q} \times 100\% \qquad (1)$$

Here, V_{HS} is the volume of the headspace in the first chamber of the electrolysis cell, V_{m} = 24.5 L mol^{-1} is the molar volume of gas at 25 °C and 1.0 atm, C is the volume percent of the CO or H_2 product detected by GC, n = 2 is the number of electrons passed per reaction for the production of CO or H_2, F = 96,485 C mol^{-1} is Faraday's constant, and Q is the amount of charge passed during the CPE measurement.

UV-Vis Spectroscopy

0.01 mM CoPc/DMF and CoPc(L)/DMF solutions were analyzed using PerkinElmer Lambda 265 UV-Vis Spectrophotometer with fast mode and baseline correction. The 0.01 mM solutions were prepared by diluting the corresponding 0.05 mM CoPc/DMF and CoPc(L)/DMF deposition solutions described above.

Density Functional Theory Calculations

All quantum-chemical calculations utilized density functional theory as implemented in the Q-Chem 5.1 software package.[55] The B3LYP density functional with the 6-31G** basis function was employed for

the gas-phase geometry optimization of the CoPc(L) systems. Single point calculations were employed to calculate the orbitals energies using B3LYP in combination with 6-311+G** basis on all atoms except def2-TZVP on the Co atom. To obtain the binding energy (BE) of CO_2 to the neutral and reduced CoPc(L) complexes structures were optimized with ωB97X-D and the 6-31G** basis, which accurately captures non-covalent interactions.[56] In the optimization of the reduced CoPc(L) complexes, the axial coordinating ligands were fixed in the XY plane to prevent π-stacking interactions between the ligand and the phthalocyanine rings. The reported energies were obtained using ωB97X-D and the 6-31+G** basis to better describe negatively charged ions.[38] Solvation energies were calculated using SMD[57] to model the implicit water solvent effect.

The Absolutely Localized Molecular Orbital-Charge Transfer Analysis (ALMO-CTA)[58] was used quantify electron donation within the CoPc unit and its ligands. The systems were divided into two fragments to study the forward charge transfer from: (1) ligands to the CoPc, (2) five-coordinate CoPc(L) complexes to the CO_2 adduct, and (3) five-coordinate complexes to the protonated CO_2 adduct. Reported forward CTA terms for neutral, reduced, CO_2 adsorbed CoPc(L) are obtained at the ωB97X-D/def2-SVP level of theory, while the protonated CO_2 adduct intermediate was obtain with B3LYP/def2-SVP. Additionally, the forward charge transfer from the reduced CoPc(L) species to the CO_2 adduct was calculated to obtain quantitative insight on the catalytically active species nucleophilic capacities.

RESULTS AND DISCUSSION

The core hypothesis we are testing in this study is that axial coordination of ligands L to CoPc makes the Co center more nucleophilic in the resulting CoPc(L) complexes, and that this increased nucleophilicity translates into an increase in activity for the CO_2RR compared to the four coordinate CoPc. A corollary to this hypothesis is that the nucleophilicity of the Co center in CoPc(L), and therefore the

CO_2RR activity, should be correlated to the σ-donor strength of the axial ligand. To test this hypothesis, we have conducted a combined experimental and computational study that explores how the catalytic activity and electronic structure of CoPc(L) changes as we modulate the σ-donor strength of L.

Effect of σ-donor Strength of Axial Ligands on CO_2RR Activity by CoPc(L)

To experimentally quantify the relative σ-donor strength of the axial ligands in CoPc(L) catalysts, we measured how axial ligation influences the λ_{max} of the Q band of CoPc(L). For the four-coordinate CoPc complex, the measured Q band has λ_{max} = 659 nm (Figure S1). When adding an axial ligand L to form CoPc(L), there is a red shift in the λ_{max} of the Q band attributed to the increased electron density on the central metal atom,[49,59-61] and the extent of the red shift should be directly correlated to the electron-donating ability of the ligand L (Figure S1).[61] The λ_{max} of the red-shifted Q bands for CoPc(L) solutions with axial ligands L1-L8 are shown in Figure 3. The shift in the Q-band is consistent with the postulated ordering of the σ-donor strength of the ligands L1-L8 shown in Figure 2.

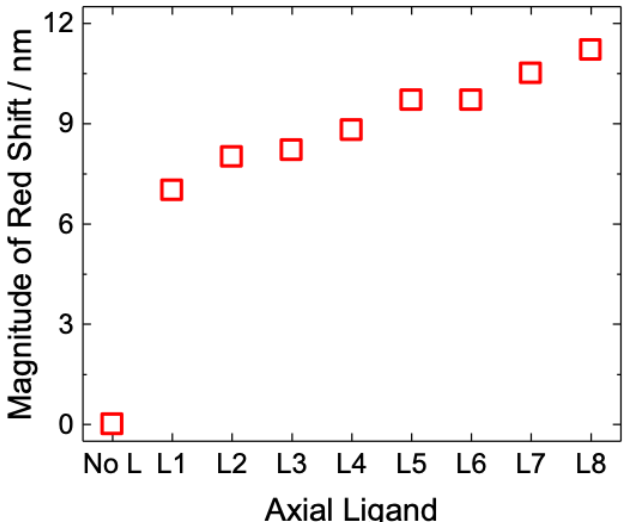

Figure 3. Magnitude of the red shift of the Q-band for solutions of CoPc(L) with axially-coordinated ligands L1-L8 compared to the λ_{max} = 659 nm of the CoPc without any axially-coordinated ligand (No L).

To investigate the influence of σ-donor strength of the axial ligand on CO_2RR activity, we evaluated the CO_2RR activity physisorbed CoPc(L) catalysts on edge-plane graphite (EPG) surfaces using rotating disk electrode voltammetry (RDEV) at 1600 rpm and 1 mV s^{-1} scan rate. The RDEV measurements were conducted at 1600 rpm and 1 mV s^{-1} scan rate. This scan rate is slow enough to ensure steady-state behavior at the electrode surface, and the rotation rate is sufficiently fast to aid in product removal and limit bubble formation from evolved CO and H_2 at the electrode surface. The resulting average RDEVs of CoPc, CoPc(L1) and CoPc(L8) for the CO_2RR are shown in Figure 4, and the average RDEVs of all complexes are shown in Figure S2. To confirm that the RDEV measurements are a true measure of steady state behavior, a series of rotating disk electrode chronoamperometric (RDE-CA) steps were measured for each catalyst (Figure S2). In these experiments, the potential was held constant at given applied potentials for 2 min at 1600 rpm rotation rate, and the current was allowed to decay to a steady state value. Average steady-state currents for the CO_2RR by each CoPc(L) complex investigated as determined from RDE-CA

measurements show good agreement when overlaid with the RDEV measurements (Figure 4), suggesting that the RDEV measurements are valid approximations of steady-state behavior.

For each CoPc(L) complex investigated, there is a plateau in the catalytic RDEV at ~ –1.25 V vs. SCE, and we attribute this plateau current to the maximum CO_2RR activity under the experimental conditions. Therefore, the activity and selectivity at –1.25 V vs. SCE was used as the primary metric to compare the CO_2RR performance for the CoPc(L) catalysts. The average current densities measured from the catalytic RDE-CA measurements are summarized in Table S2. A plot of the catalytic current density at −1.25 V for each CoPc(L) catalyst as a function of the magnitude of the red shift of the complexes' Q bands, a proxy for the σ-donor strength of the axial ligands, is shown in Figure 5a. As the σ-donor strength increases and the magnitude of the red shift increases, there is a corresponding increase in the catalytic current density. This activity trend is consistent with our hypothesis that increasing the σ-donor strength of the axial ligand in CoPc(L) correspondingly increases the nucleophilicity of the Co center, facilitating CO_2 activation and reduction.

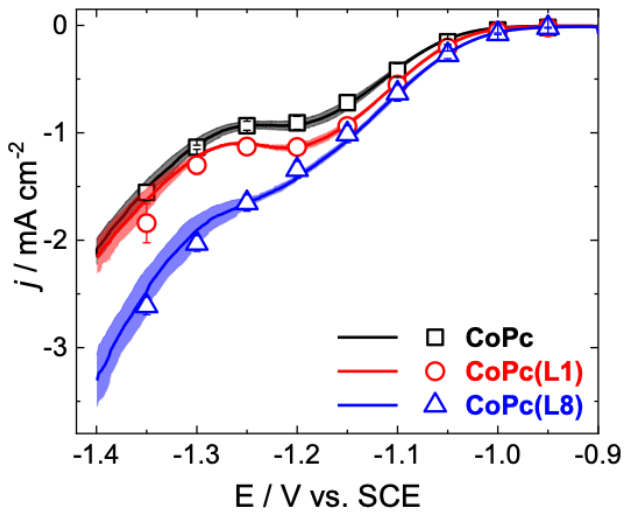

Figure 4. (a) Rotating disk electrode voltammograms (RDEVs) of the CO2RR by CoPc, CoPc(L1), and CoPc(L8) catalysts at 1 mV s-1 scan rate and 1600 rpm in CO2-saturated pH 5 phosphate solutions. The solid lines represent the averages RDEVs from at least three measurements on independently prepared samples, and the shaded region represents the standard deviation for these measurements. The average results of 2 min rotating disk electrode chronoamperometric (CA) steps from at least three measurements on independently prepared samples are shown by open symbols, and the error bars represent standard deviations for these measurements. The close overlay of the RDEV and CA data suggests that the RDEV measurements are a good approximation of steady-state conditions.

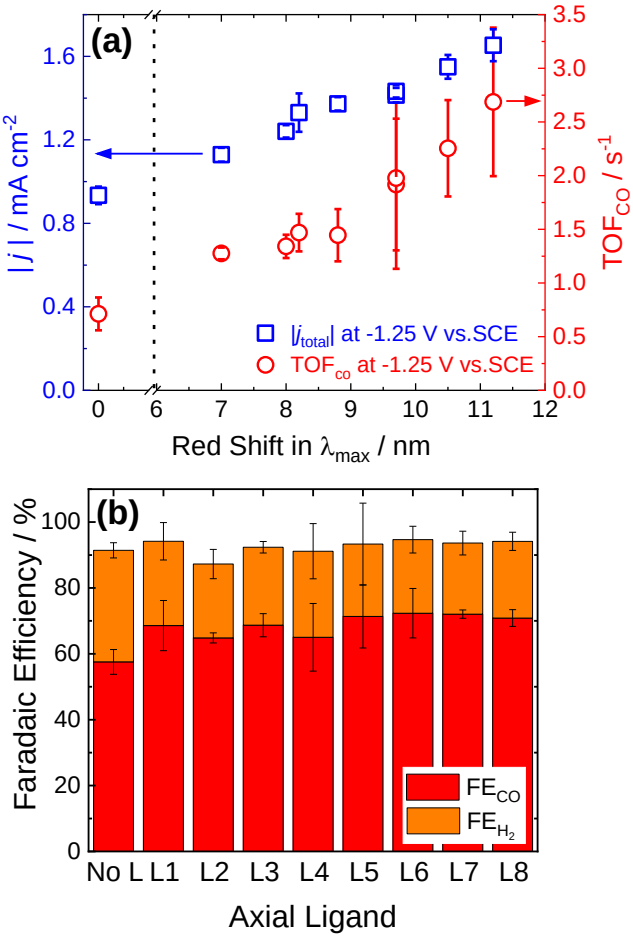

Figure 5. (a) A plot of the absolute value of the average current density from RDE-CA measurements (left y-axis) and turnover frequency, TOF_{CO}, from the CPE measurements (right y-axis) at −1.25 V vs SCE as a function of the red shift in λ_{max} for CoPc(L) which is related to the σ-donor ability of the axial ligands, L. Note the vertical dotted line highlights a break in the x-axis at λ_{max} = 1 nm, and the scale continues after the break at λ_{max} = 6 nm. (b) A plot of the average Faradaic efficiencies for CO and H_2 production from CPE measurements at −1.25 V vs SCE. For both (a) and (b), the data shown are averages from at least three experiments on independently prepared samples, and the error bars represent standard deviations.

Controlled potential electrolysis (CPE) were performed at –1.25 V vs. SCE to assess Faradaic efficiencies for CO_2 reduction to CO (FE_{CO}) by CoPc and CoPc(L) modified electrodes. Electrolyses were conducted in a sealed electrochemical cell in CO_2 atmosphere for 2 h, and CO and H_2 evolved were quantified from headspace analysis using gas chromatography. Representative examples of the CPE current traces are shown in Figures S3-S11 for each catalyst, and the resulting Faradaic efficiencies for H_2 (FE_{H2}) and CO (FE_{CO}) generation are summarized in Figure 5b and Table S1 . In general, the only products produced were CO and H_2. All CoPc(L) catalysts reduce CO_2 to CO with $FE_{CO} \approx 70\%$, and CoPc with no axial ligand produces CO with $FE_{CO} \approx 60\%$. Note that control CPE experiments of the EPG background under identical conditions showed only H_2 as the sole product, confirming that the adsorbed CoPc(L) complexes are the active species for the CO_2RR. The increased FE for CoPc(L) compared to CoPc is consistent with our previous findings that axial coordination of ligands such as pyridine to the CoPc complex facilitate CO_2 coordination by shifting the rate determining step from an initial CO_2 binding step to a subsequent protonation event.[18] The fact that all the CoPc(L) systems show the same FE for CO production suggests that this change in the rate-determining step upon axial coordination occurs for all CoPc(L) systems investigated independent of σ-donor ability of the axial ligand. A plot of the electrocatalytic turnover frequencies for CO production (TOF_{CO}) determined from the CPE measurements as function of the magnitude of the red shift of the complexes' Q bands shows increasing activity with increasing σ-donor strength of the axial ligand, qualitatively similar to the trend observed from the RDE-CA measurements (Figure 5a).

Note that there rising region in the RDEV and RDE-CA measurements in Figure 4 after the plateau at potentials < −1.25 V is attributed to the onset of competitive HER from the EPG electrode, which occurs at ∼−1.3 V vs SCE (Figure S12). CPE experiments conducted at −1.35 V for CoPc, CoPc(L3), and

CoPc(L8) show a large increase in H_2 production with $FE_{H2} \geq 75\%$, consistent with the postulated increase in the HER at these more negative potentials (Table S3).

The Effect of σ-donor Strength of Axial Ligands on Electronic Structure of CoPc(L)

To better understand the influence of the σ-donor strength of axially-coordinating ligands on the electronic structure of CoPc(L), density functional theory (DFT) was used to examine molecular orbitals for the various CoPc(L) complexes. The orbitals with primarily dz^2 character (dz^2-MOs) and the highest occupied molecular orbitals (HOMOs) for CoPc and CoPc(L) are shown in Figure 6 for CoPc, CoPc(L1), and CoPc(L8), and for all complexes in Figure S13. For all CoPc and CoPc(L) complexes, the HOMOs are primarily composed of π-orbitals of the Pc rings. The dz^2 orbital of CoPc is relatively low energy (i.e. the HOMO−5 orbital), but upon axial ligation it increases in energy by ~2.1 eV and becomes the HOMO−1 for CoPc(L). The relative increase of the dz^2 orbital energy increases with increasing σ-donor strength of L as shown in Figure 7a and summarized in Table S4.

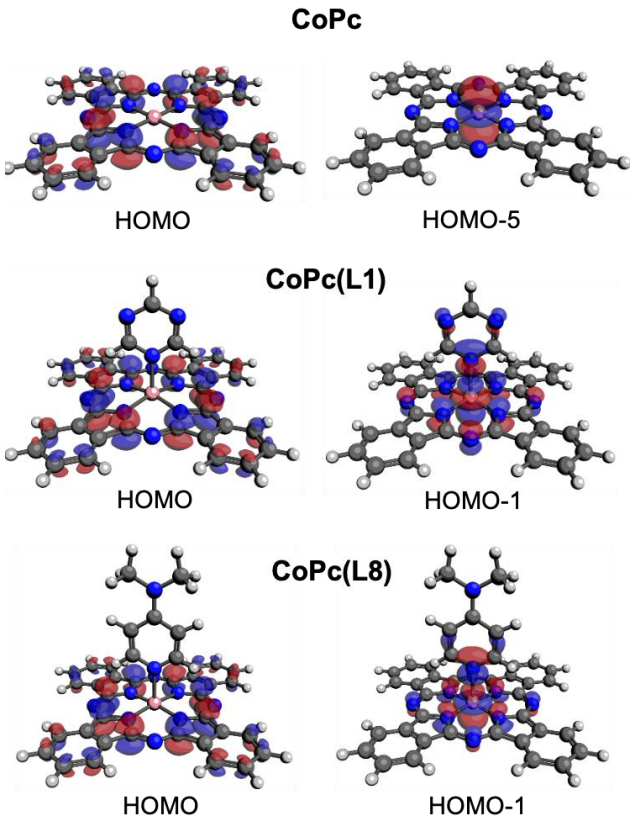

Figure 6. Graphical representations of the HOMO (left) and dz^2 orbitals (right) for CoPc, CoPc(L1), and CoPc(L8). Calculated charge distributions (red and blue shaded orbitals) are based on DFT calculations (pink ball = Co, blue ball = N, grey ball = C, white ball = H). Isovalue is 0.10 a.u.

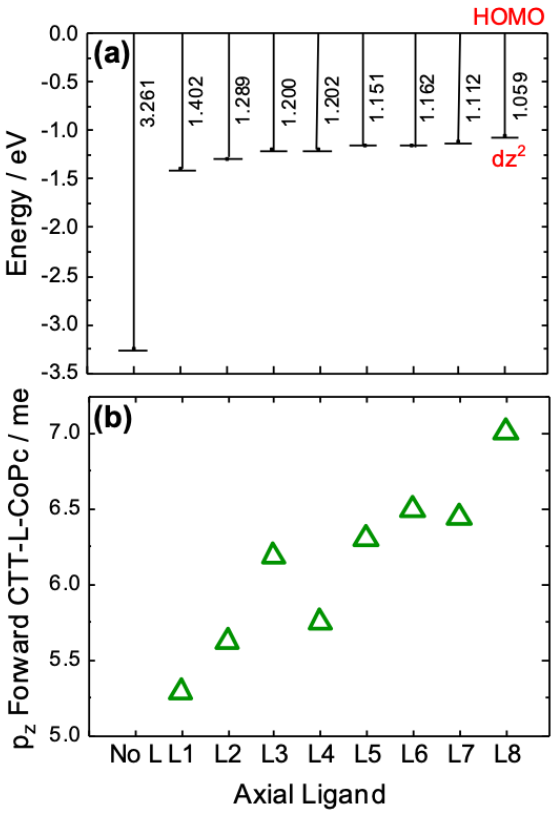

Figure 7. (a) Calculated energy differences between the HOMO and dz^2-MO for CoPc(L) with various axial ligands L. (b) The forward charge transfer term from the ligand L nitrogen p_z to the CoPc complex (CTT-L-CoPc) from ALMO-CTA. CTT-L-CoPc are in millielectrons (me).

Charge transfer analysis (see computational details) determined the primary interaction between the CoPc complex and axial ligand L in CoPc(L) is σ-donation from the p_z orbital of the coordinating N atom to the dz^2 orbital of the Co atom. This interaction between N p_z and Co dz^2 accounts for > 80% of the forward charge transfer between the ligands L and the CoPc. The second significant interaction is a π-interaction between the p_x orbitals of the conjugated C atoms in L and the p orbitals of the outer C-N-C atoms in the Pc, accounting for ~10% of the forward charge transfer. The additional electron density on the Co center compared to the parent complex CoPc suggests that the Co will have increased

nucleophilicity. Moreover, the magnitude of the forward charge transfer term from the ligand L to the CoPc complex (CTT-L-CoPc) increases with increasing σ-donor strength of L as shown in Figure 7b. The DFT findings are therefore consistent with the UV-Vis measurements showing a red shift in the Q-band as a function of σ-donor strength of L (Figure 3 and Figure S14). These results support the hypothesis that axial coordination increases the energy of the Co dz^2 orbital, and thus the nucleophilicity of the Co center, in proportion to the σ-donor strength of the axial ligand.

Mechanistic Implications of Axial Coordination from First Principles Calculations

The above DFT analysis focused on the electronic structure of the uncharged CoPc(L) species serves as a baseline for understanding the influence of axial coordination on the electronic structure. To best inform the electrocatalytic mechanism of the CoPc(L) system, it is important to understand the influence of axial coordination on the catalytically-active reduced CoPc and CoPc(L) species. Here, we introduce probable mechanisms for CO_2RR by CoPc in order to identify relevant catalytically active species for further computational study.

Although the mechanism for the CO_2RR by CoPc is likely condition-dependent and remains an active point of discussion,[21,22,25,39] two mechanisms have emerged that are largely consistent with experimental measurements in aqueous solution and are depicted in Scheme 1. In Mechanism 1 (Scheme 1a), the active species for CO_2 activation is the singly-reduced $[CoPc]^-$ intermediate, which can either coordinate and reduce CO_2 to generate CO in the CO_2RR pathway or undergo reductive protonation to generate H_2 along the competitive HER pathway. In Mechanism 2 (Scheme 1b), CoPc is reduced by $2e^-$ and protonated once (presumably on the Pc ring) to form $[CoPcH]^-$. This species is the selectivity-determining intermediate that can either react with another H^+ to form H_2 in an HER pathway or react with CO_2 to form the CO_2 adduct $[CoPcH\text{-}CO_2]^-$. The latter intermediate undergoes a putative intramolecular H^+ transfer from the

Pc ring to the CO_2 adduct followed by a subsequent solution protonation step to eventually generate CO. Both mechanisms are consistent with KIE studies that show axial coordination changes the rate determining step from the initial CO_2-coordination event (step i) for CoPc to a subsequent protonation event (step ii) for CoPc(L).[18]

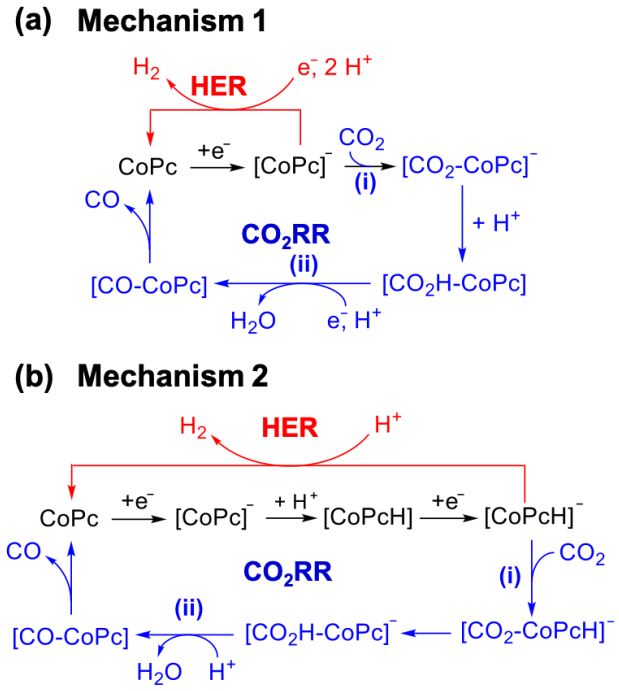

Scheme 1. Two proposed mechanisms for the CO_2RR by CoPc. (a) In Mechanism 1, CO_2 coordination occurs at the singly-reduced catalyst.[25,39] (b) In Mechanism 2, CO_2 coordination occurs at the doubly-reduced and singly-protonated catalyst.[15,21,22] Both mechanisms are consistent with KIE studies that show a change in the rate-determining step upon axial coordination from CO_2 coordination (step i) to a subsequent protonation event (step ii).[18] Postulated pathways for competitive HER are shown in red for each mechanism.

To help distinguish between the two proposed mechanisms for CO_2RR by CoPc(L) catalysts, we compared the experimental activity measurements to computed frontier orbitals, CO_2 binding energies (BE), and charge transfer terms (CTT) for the CoPc(L) CO_2 adduct. We propose that a close correlation of increasing BE and CTT for the pertinent mechanistic intermediates in Mechanisms 1 or 2 with increasing σ-donor strength of the axial ligand suggests that the mechanism is consistent with experimental results (Figure 8). Such an agreement would then correlate BE and CTT of CoPc(L) to the CO_2 adduct with the measured catalytic activity, which also increases with σ-donor strength of the axial ligand. These first-principles studies will relate the electronic properties of CoPc(L) to the measured electrocatalytic activity for the CO_2RR.

The orbital ordering for the intermediates preceding CO_2 coordination was examined for each mechanism, $[CoPc(L)]^-$ for Mechanism 1 and $[CoPcH(L)]^-$ for Mechanism 2 (Figure 9 a,b). In the case of the singly-reduced $[CoPc]^-$ active species from Mechanism 1, the dz^2-MO is HOMO-3 (Figure 9a). Upon axial coordination to reach $[CoPc(L)]^-$, the dz^2-MO increases in energy to become the HOMO for all L1-L8 (Figure 9a, S16). This shows that the dz^2-MO of $[CoPc(L)]^-$ is better poised to activate and coordinate the electrophilic C of CO_2 compared to that of $[CoPc]^-$, assuming Mechanism 1 is the operative mechanism for CO_2RR.

For the active species from Mechanism 2, $[CoPcH]^-$, the dz^2-MO is also a buried HOMO-3 similar to the intermediate in Mechanism 1 (Figure 9b). For the axially-coordinated $[CoPcH(L)]^-$ active species, the dz^2-MO becomes HOMO-2 and the HOMO is still composed primarily of π-orbitals of the Pc rings (Figure 9b, S18). These calculations suggest that Co center of $[CoPcH(L)]^-$ is more nucleophilic than that of $[CoPcH]^-$, but that the buried dz^2-MO of $[CoPcH(L)]^-$ is not as well positioned energetically to interact with CO_2 compared to the singly-reduced $[CoPc(L)]^-$ in Mechanism 1. This may suggest that Mechanism 2 is a less likely mechanism for the CO_2RR compared to Mechanism 1.

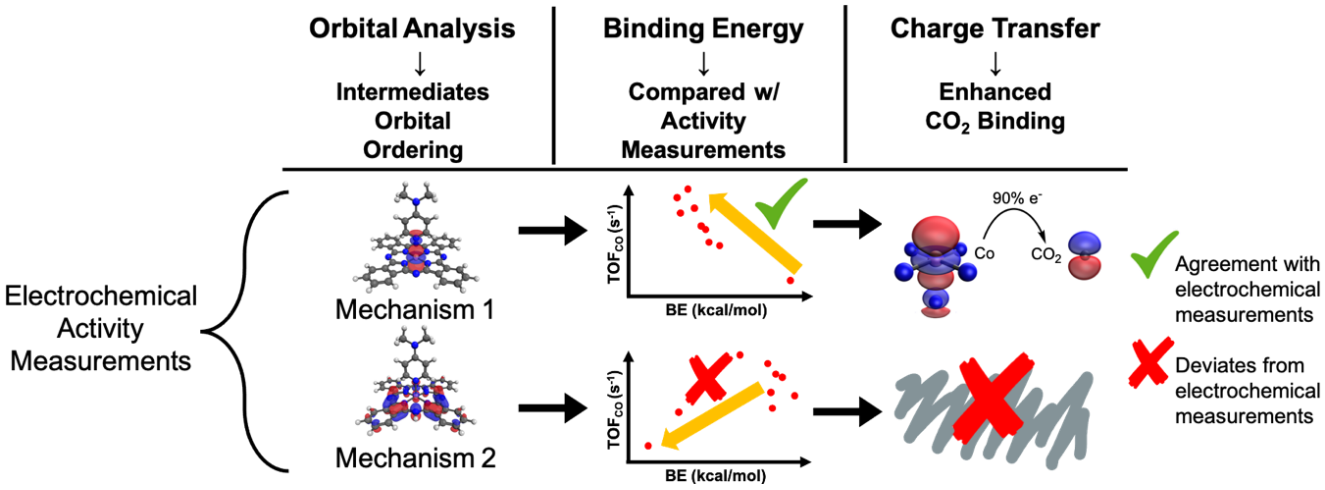

Figure 8. Overview of DFT analysis for the proposed CO_2RR mechanisms for CoPc(L) catalysts. These calculations were used to look for trends that can explain the comparative measured electrocatalytic activities for the CoPc(L) systems. First, we determined the HOMO orbital character for the postulated catalytically-active intermediates. Next, we compared trends in the CO_2 binding energy for the intermediates in Mechanism 1 and 2 to trends in the measured catalytic activities (TOF_{CO}). Finally, we measured the influence of the σ-donor strength of the axial ligands L on the extent of charge transfer between CoPc(L) and the CO_2 adducts in the relevant intermediates for both mechanisms. If we assume that CO_2-binding thermodynamically-controls CO_2RR activity and the energy of the mechanistically-pertinent CoPc(L)-CO_2 intermediates influence catalytic turnover, then these analyses are more consistent with Mechanism 1 being the operative mechanism for CO_2RR under our experimental conditions.

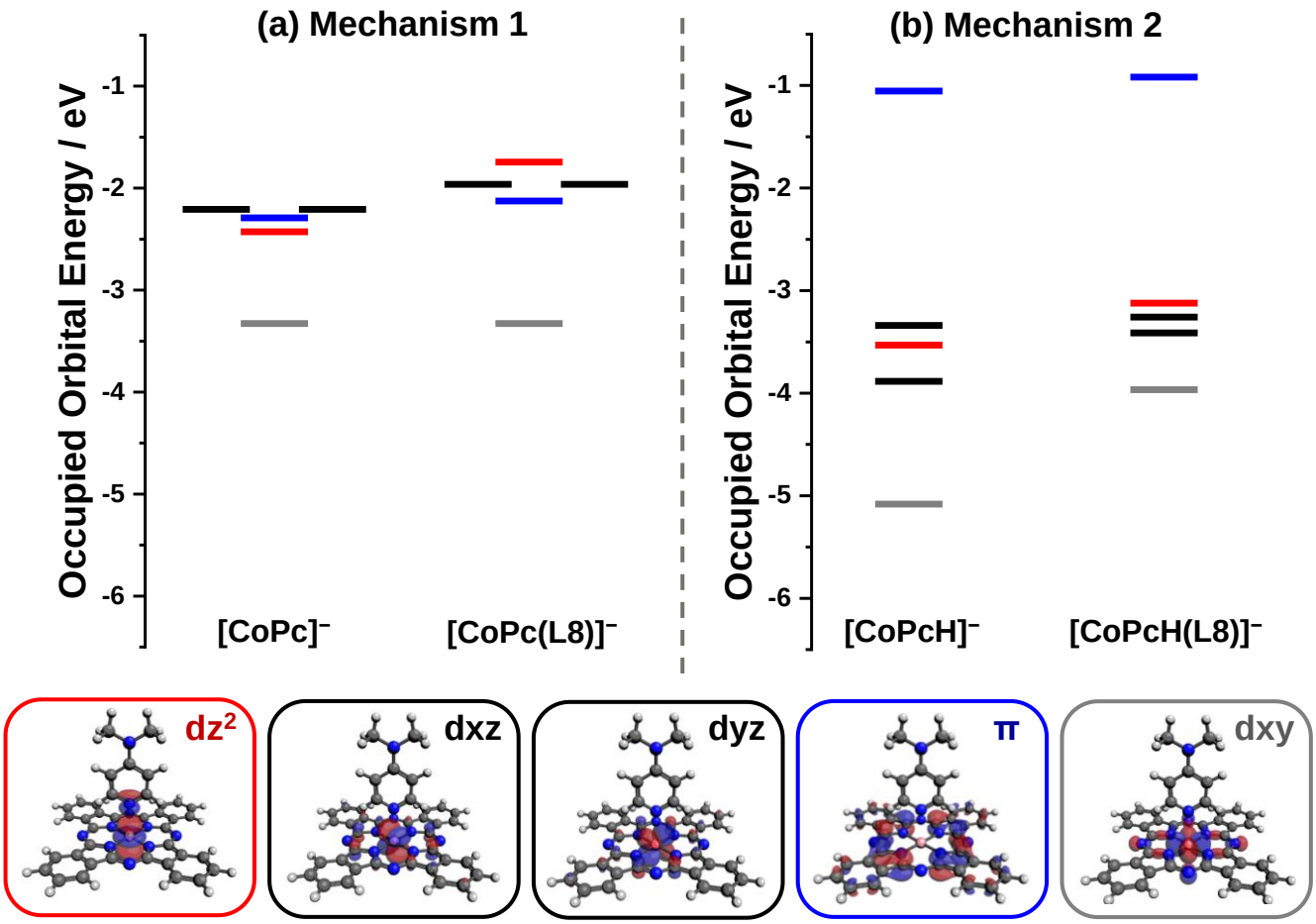

Figure 9. Energies of the occupied frontier molecular orbitals obtained for the singlet state singly reduced $[CoPc(L)]^-$ and the doublet state of the doubly reduced, singly protonated $[CoPcH(L)]^-$ with and without axially coordinating L ligands. The colors of the energy levels correspond to the specific molecular orbitals: red is dz^2, black is dxz and dyz, grey is dxy, and blue is the π orbital of the Pc ring. Graphical representations of the molecular orbitals for $[CoPc(L8)]^-$ with color-coordinated labels are shown for reference, and the graphical representations for the other orbitals are shown in Figures S15 and S17. Summaries of the orbital energies and assignments are listed in Table S5 and Table S6.

The CO_2 coordination via the $[CoPc(L)\text{-}CO_2]^-$ and $[CoPc(L)\text{-}CO_2H]^-$ intermediates were then evaluated based on the assumption that these intermediates are the thermodynamically controlling species prior to the rate-limiting CO_2 conversion steps. According to Mechanism 1, CO_2 coordination should occur at the singly-reduced $[CoPc(L)]^-$. The computed BE of CO_2 in $[CoPc(L)\text{-}CO_2]^-$ is much more negative (larger magnitude) than that of the comparable CO_2-adduct of the four-coordinate CoPc species in $[CoPc\text{-}CO_2]^-$. This suggests that axial coordination facilitates the binding of CO_2 at the singly-reduced state in Mechanism 1. This is consistent with our experimental observations that show axial coordination changes the rate-determining step from CO_2 coordination to a subsequent mechanistic step.[18] Moreover, the BE of the CO_2 adduct increases with σ-donor ability of L as measured by the red-shift in the Q-band for the CoPc (L) complex (Figure 11a). In addition, there is a direct correlation between BE and TOF_{CO} for the CoPc(L) complexes (Figure 11c). The DFT and experimental observations suggest that axial coordination by strong σ-donor ligands facilitates CO_2 coordination, increasing the rate of CO_2 reduction to CO by the CoPc(L) complexes.

According to Mechanism 2, CO_2 coordination should occur at the doubly-reduced singly-protonated $[CoPcH(L)]^-$, producing $[CoPc(L)\text{-}CO_2H]^-$. However, unlike with Mechanism 1, there is no clear correlation between the BE of the CO_2 adduct in the intermediate $[CoPc(L)\text{-}CO_2H]^-$ with either the σ-donor ability of L (Figure 11b) or TOF_{CO} (Figure 11d). Overall, these results suggest that Mechanism 2 is less likely than Mechanism 1 to be operative under our experimental conditions.

To provide further understanding of the observed trends in BE, the extent of CTTs from the reduced CoPc(L) species to the CO_2 adducts were computed. In the case of Mechanism 1, the primary interaction contributing to the charge transfer between the complex and CO_2 is the σ-donation from the Co dz^2 to the p_z orbitals in the CO_2 adduct (Table S7). For the intermediate $[CoPc(L)\text{-}CO_2]^-$, there is a general increase in CTT between $[CoPc(L)]^-$ and CO_2 with increasing σ-donor strength of the ligand L (Figure 12a), and

this increased CTT is correlated to the increased activity for the CO_2RR (Figure 12b). The extent of CTT for the $[CoPc(L)]^-$ species to the protonated CO_2 adducts for $[CoPc(L)\text{-}CO_2H]^-$ was calculated for Mechanism 2 (Table S8), but there was a lack of correlation between the CTT and the experimentally-measured activity (Figure S21). The trends in CTT to CO_2 with L were less predictive of electrocatalytic activity for the key intermediate of Mechanism 2 compared to Mechanism 1.

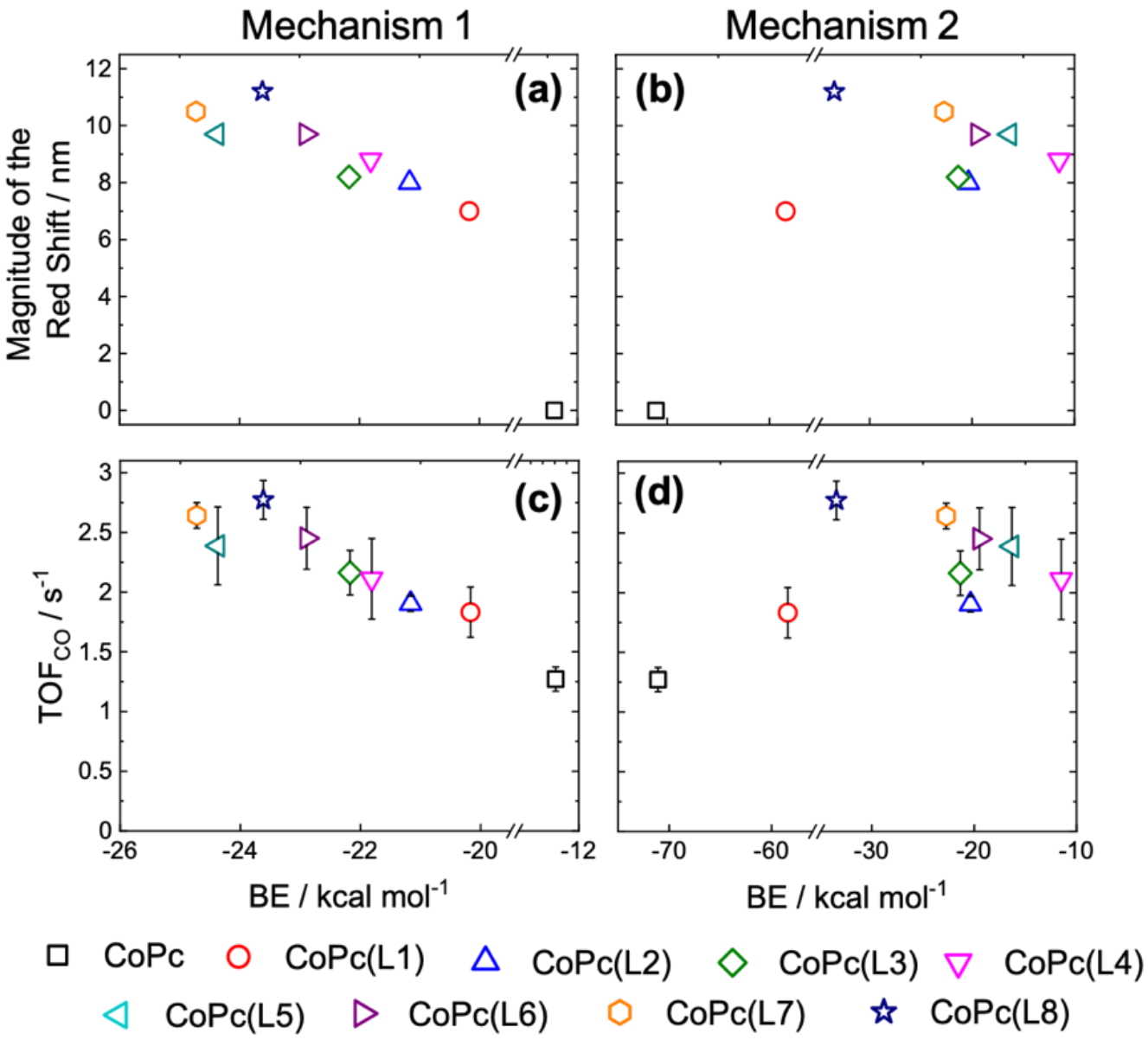

Figure 11. (a) The magnitude of the red shift in λ_{max} of the Q-band for the CoPc(L) complex (related to the σ-donor ability of L) is plotted versus the binding energy (BE) of CO_2 adduct in the $[CoPc(L)\text{-}CO_2]^-$ intermediate. b) The magnitude of the red shift in λ_{max} versus BE of the CO_2H adduct in $[CoPc(L)\text{-}CO_2H]^-$. (c-d) Same as (a) and (b), respectively, but with y-axis as Turnover Frequency for CO (TOF_{CO}). TOF_{CO} measurements here were determined by multiplying the RDE-CA measurements at −1.25 V vs SCE by the FE_{CO} from the CPE measurements at −1.25 V. Graphical representations for the HOMOs and orbitals showing the interaction between the complex and CO_2 for $[CoPc(L)\text{-}CO_2]^-$ and $[CoPc(L)\text{-}CO_2H]^-$ are shown in Figures S19 and S20, respectively.

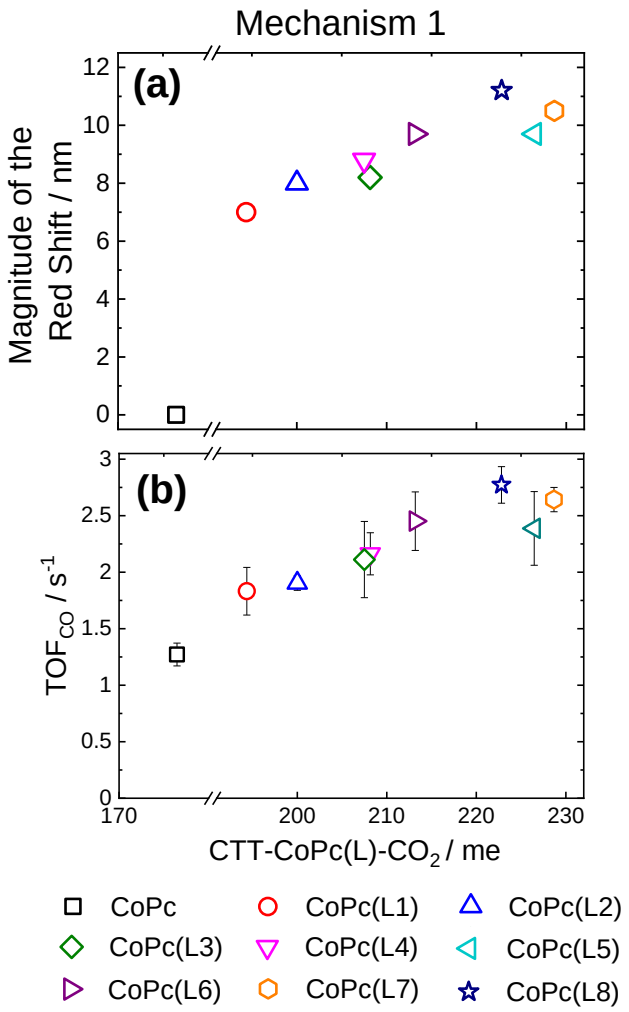

Figure 12. (a) The magnitude of the red shift in λ_{max} of the Q-band plotted versus the forward charge transfer term from the singly-reduced CoPc(L) to the coordinated CO_2 adduct in the $[CoPc(L)\text{-}CO_2]^-$ intermediates (CTT-CoPc(L)-CO_2) (b) The activity as measured by the Turnover Frequency (TOF_{CO}) for the CoPc(L) complexes is plotted versus the same CTT. CTT were from ALMO-CTA analysis, and the units are millielectrons (me). TOF_{CO} here were determined by multiplying the RDE-CA measurements at −1.25 V vs SCE by the FE_{CO} from the CPE measurements at −1.25 V.

CONCLUSIONS

It has been previously shown that axial ligation of the CoPc complex by either a coordination ligand such as pyridine (L3) or a coordinating polymer such as P4VP results in increased activity and selectivity for the CO_2RR to CO in aqueous phosphate solutions.[17,18,21,22] We hypothesized that axial coordination increases the energy of the dz^2 orbital, the orbital most likely involved in CO_2 coordination, and that this higher energy dz^2 orbital facilitates CO_2 reduction. The combined electrochemical and computational study reported here provides strong support for this hypothesis. We investigated the activity for the CO_2RR by a series of CoPc(L) complexes, where L increases in σ-donor strength from the relatively weak σ-donor triazine (L1) to the comparatively strong sigma donor 4-dimethylaminopyridine (L8). Our studies showed a correlation between the increasing σ-donor strength of L and the increased catalytic activity of the resulting CoPc(L) complexes for the CO_2RR. Using DFT analysis, we also showed that the relative energy of the dz^2 orbital increases with increasing σ-donor ability of the axial ligand, and that Co dz^2 orbital is the primary orbital that interacts with CO_2 in the reduced CoPc(L)-CO_2 intermediates. These findings suggest that the observed increases in CO_2RR activity for CoPc(L) with increasing σ-donor ability of L are correlated with the increased relative energy of the Co dz^2 orbitals in the CoPc(L) complexes.

We also compared first-principles calculations of CO_2 Binding Energy (BE) and Charge Transfer terms (CTT) between the CoPc(L) and CO_2 for active intermediates in two proposed mechanisms for the CO_2RR by CoPc. We showed that, in the case of Mechanism 1, where CO_2 binding occurs after the first reduction of the CoPc(L) system, the CTT and BE terms for the singly-reduced $[CoPc(L)\text{-}CO_2]^-$ intermediate increased with increasing σ-donor ability of the ligand. The result is a direct correlation of the calculated CTT and BE terms with the experimentally measured CO_2RR activity, suggesting that Mechanism 1 is a possible operative mechanism for this reaction. However, for Mechanism 2, where CO_2 binding occurs after the second reduction and first protonation of the CoPc(L) system, there was a less

clear correlation between the calculated CTT and BE terms for the doubly-reduced, singly protonated $[CoPc(L)\text{-}CO_2H]^-$ intermediate and the σ-donor ability of the ligand. Consequently, there was no clear correlation between the BE and CTT terms for Mechanism 2 and the measured catalytic activity, suggesting that Mechanism 2 is less likely to be an operative mechanism. From these studies, we conclude that Mechanism 1 is more likely than Mechanism 2 to explain the CO_2RR by the CoPc and CoPc(L) systems under our experimental conditions.

Overall, our studies provide strong support that axial ligation increases the energy of the dz^2 orbital in the CoPc(L) complexes, the extent of this increase in the dz^2 orbital energy is dependent on the σ-donor strength of the axial ligand, and that this increased dz^2 orbital energy for the CoPc(L) complexes is likely correlated to the observed increase in activity for the CO_2RR. We believe that these studies illustrating the influence of axial coordination on electronic structure and electrocatalytic activity provide important design considerations for future macrocyclic MN_4-based electrocatalytic systems.

ACKNOWLEDGEMENTS

We thank Weijie Feng, Matthew D. Hannigan, and Alan E. Rask for useful discussions regarding computational studies. This work was supported by an NSF-CAREER grant (CHE-1751791). Y. L. was partially supported by a Rackham One-Term Dissertation Fellowship from the University of Michigan. K. E. R. C. was partially supported by a GEM Full Fellowship from the National GEM Consortium. T. L. S. was partially supported by the National Science Foundation Graduate Research Fellowship Program (DGE 1256260).

ASSOCIATED CONTENT

Supporting Information. The Supporting Information is available free of charge.

- UV-Vis spectra; representaitve rotating disk voltammograms and rotating disk chronomamperometric steps; summary of results from controlled-potential electrolysis experiments; calculated highest occupied molecular orbitals, dz^2 orbitals, and other relevant molecular orbitals for CoPc and CoPc(L) species.
- The *XYZ* coordinates of the structures used in the DFT calculations for all species investigated: CoPc, CoPc(L), $[CoPc]^-$, $[CoPc(L)]^-$, $[CoPc\text{-}CO_2]^-$, $[CoPc(L)\text{-}CO_2]^-$, $[CoPcH]^-$, $[CoPcH(L)]^-$ $[CoPc\text{-}CO_2H]^-$ and $[CoPc(L)\text{-}CO_2H]^-$; L = L1 to L8.

AUTHOR INFORMATION

Author Information:

*Email for P. M. Z.: paulzim@umich.edu

*Email for C. C. L. M.: cmccrory@umich.edu

Author Contributions:

#K.E.R.C. and Y.L. contributed equally to this work.

ORCID

Kevin E. Rivera Cruz: 0000-0001-6690-1571

Yingshuo Liu: 0000-0003-4780-8384

Taylor L. Soucy: 0000-0002-0090-6721

Paul M. Zimmerman: 0000-0002-7444-1314

Charles C. L. McCrory: 0000-0001-9039-7192

Notes:

The authors declare no competiting financial interest.

REFERENCES

(1) Roy, S. C.; Varghese, O. K.; Paulose, M.; Grimes, C. A. "Toward Solar Fuels: Photocatalytic Conversion of Carbon Dioxide to Hydrocarbons," *ACS Nano* **2010**, *4*, 1259-1278. http://dx.doi.org/10.1021/nn9015423

(2) Whipple, D. T.; Kenis, P. J. A. "Prospects of CO2 Utilization via Direct Heterogeneous Electrochemical Reduction," *J. Phys. Chem. Lett.* **2010**, *1*, 3451-3458. http://dx.doi.org/10.1021/jz1012627

(3) Inglis, J. L.; MacLean, B. J.; Pryce, M. T.; Vos, J. G. "Electrocatalytic pathways towards sustainable fuel production from water and CO_2," *Coord. Chem. Rev.* **2012**, *256*, 2571-2600. http://dx.doi.org/10.1016/j.ccr.2012.05.002

(4) Kondratenko, E. V.; Mul, G.; Baltrusaitis, J.; Larrazábal, G. O.; Pérez-Ramírez, J. "Status and perspectives of CO2 conversion into fuels and chemicals by catalytic, photocatalytic and electrocatalytic processes," *Energy Environ. Sci.* **2013**, *6*. http://dx.doi.org/10.1039/c3ee41272e

(5) Martín, A. J.; Larrazábal, G. O.; Pérez-Ramírez, J. "Towards sustainable fuels and chemicals through the electrochemical reduction of CO2: lessons from water electrolysis," *Green Chem.* **2015**, *17*, 5114-5130. http://dx.doi.org/10.1039/C5GC01893E

(6) Shaner, M. R.; Atwater, H. A.; Lewis, N. S.; McFarland, E. W. "A comparative technoeconomic analysis of renewable hydrogen production using solar energy," *Energy Environ. Sci.* **2016**, *9*, 2354-2371. http://dx.doi.org/10.1039/C5EE02573G

(7) Nocera, D. G. "Solar Fuels and Solar Chemicals Industry," *Acc. Chem. Res.* **2017**, *50*, 616-619. http://dx.doi.org/10.1021/acs.accounts.6b00615

(8) Senftle, T. P.; Carter, E. A. "The Holy Grail: Chemistry Enabling an Economically Viable CO_2 Capture, Utilization, and Storage Strategy," *Acc. Chem. Res.* **2017**, *50*, 472-475. http://dx.doi.org/10.1021/acs.accounts.6b00479

(9) Spurgeon, J. M.; Kumar, B. "A comparative technoeconomic analysis of pathways for commercial electrochemical CO2 reduction to liquid products," *Energy Environ. Sci.* **2018**, *11*, 1536-1551. http://dx.doi.org/10.1039/C8EE00097B

(10) Mustafa, A.; Lougou, B. G.; Shuai, Y.; Wang, Z.; Tan, H. "Current technology development for CO2 utilization into solar fuels and chemicals: A review," *J. Energy Chem.* **2020**, *49*, 96-123. http://dx.doi.org/10.1016/j.jechem.2020.01.023

(11) Crabtree, R. H. "Alternate Strategies for Solar Fuels from Carbon Dioxide," *ACS Energy Lett.* **2020**, *5*, 2505-2507. http://dx.doi.org/10.1021/acsenergylett.0c01359

(12) Verma, S.; Kim, B.; Jhong, H.-R. M.; Ma, S.; Kenis, P. J. A. "A Gross-Margin Model for Defining Technoeconomic Benchmarks in the Electroreduction of CO2," *ChemSusChem* **2016**, *9*, 1972-1979. http://dx.doi.org/10.1002/cssc.201600394

(13) Zheng, T.; Jiang, K.; Wang, H. "Recent Advances in Electrochemical CO2-to-CO Conversion on Heterogeneous Catalysts," *Adv. Mater.* **2018**, *30*, 1802066. http://dx.doi.org/10.1002/adma.201802066

(14) De Luna, P.; Hahn, C.; Higgins, D.; Jaffer, S. A.; Jaramillo, T. F.; Sargent, E. H. "What would it take for renewably powered electrosynthesis to displace petrochemical processes?," *Science* **2019**, *364*, eaav3506. http://dx.doi.org/10.1126/science.aav3506

(15) Lieber, C. M.; Lewis, N. S. "Catalytic reduction of carbon dioxide at carbon electrodes modified with cobalt phthalocyanine," *J. Am. Chem. Soc.* **1984**, *106*, 5033-5034. http://dx.doi.org/10.1021/ja00329a082

(16) Kapusta, S.; Hackerman, N. "Carbon Dioxide Reduction at a Metal Phthalocyanine Catalyzed Carbon Electrode," *J. Electrochem. Soc.* **1984**, *131*, 1511-1514. http://dx.doi.org/10.1149/1.2115882

(17) Kramer, W. W.; McCrory, C. C. L. "Polymer coordination promotes selective CO_2 reduction by cobalt phthalocyanine," *Chem. Sci.* **2016**, *7*, 2506-2515. http://dx.doi.org/10.1039/C5SC04015A

(18) Liu, Y.; McCrory, C. C. L. "Modulating the mechanism of electrocatalytic CO_2 reduction by cobalt phthalocyanine through polymer coordination and encapsulation," *Nat. Commun.* **2019**, *10*, 1683. http://dx.doi.org/10.1038/s41467-019-09626-8

(19) Liu, Y.; Deb, A.; Leung, K. Y.; Nie, W.; Dean, W. S.; Penner-Hahn, J. E.; McCrory, C. C. L. "Determining the coordination environment and electronic structure of polymer-encapsulated cobalt phthalocyanine under electrocatalytic CO_2 reduction conditions using in situ X-Ray absorption spectroscopy," *Dalton Trans.* **2020**, *49*, 16329-16339. http://dx.doi.org/10.1039/D0DT01288B

(20) Kusuda, K.; Ishihara, R.; Yamaguchi, H.; Izumi, I. "Electrochemical investigation of thin films of cobalt phthalocyanine and cobalt-4,4′,4″,4‴-tetracarboxyphthalocyanine and the reduction of carbon monoxide, formic acid and formaldehyde mediated by the Co(I) complexes," *Electrochim. Acta* **1986**, *31*, 657-663. http://dx.doi.org/10.1016/0013-4686(86)87032-3

(21) Yoshida, T.; Kamato, K.; Tsukamoto, M.; Iida, T.; Schlettwein, D.; Wöhrle, D.; Kaneko, M. "Selective electroacatalysis for CO_2 reduction in the aqueous phase using cobalt phthalocyanine/poly-4-vinylpyridine modified electrodes," *J. Electroanal. Chem.* **1995**, *385*, 209-225. http://dx.doi.org/10.1016/0022-0728(94)03762-R

(22) Abe, T.; Yoshida, T.; Tokita, S.; Taguchi, F.; Imaya, H.; Kaneko, M. "Factors affecting selective electrocatalytic CO_2 reduction with cobalt phthalocyanine incorporated in a polyvinylpyridine membrane coated on a graphite electrode," *J. Electroanal. Chem.* **1996**, *412*, 125-132. http://dx.doi.org/10.1016/0022-0728(96)04631-1

(23) Zhang, X.; Wu, Z.; Zhang, X.; Li, L.; Li, Y.; Xu, H.; Li, X.; Yu, X.; Zhang, Z.; Liang, Y.; Wang, H. "Highly selective and active CO2 reduction electrocatalysts based on cobalt phthalocyanine/carbon nanotube hybrid structures," *Nat. Commun.* **2017**, *8*, 14675. http://dx.doi.org/10.1038/ncomms14675

(24) Wu, H.; Zeng, M.; Zhu, X.; Tian, C.; Mei, B.; Song, Y.; Du, X.-L.; Jiang, Z.; He, L.; Xia, C.; Dai, S. "Defect Engineering in Polymeric Cobalt Phthalocyanine Networks for Enhanced Electrochemical CO2 Reduction," *ChemElectroChem* **2018**, *5*, 2717-2721. http://dx.doi.org/10.1002/celc.201800806

(25) Zhu, M.; Ye, R.; Jin, K.; Lazouski, N.; Manthiram, K. "Elucidating the Reactivity and Mechanism of CO_2 Electroreduction at Highly Dispersed Cobalt Phthalocyanine," *ACS Energy Lett.* **2018**, *3*, 1381-1386. http://dx.doi.org/10.1021/acsenergylett.8b00519

(26) Boutin, E.; Wang, M.; Lin, J. C.; Mesnage, M.; Mendoza, D.; Lassalle-Kaiser, B.; Hahn, C.; Jaramillo, T. F.; Robert, M. "Aqueous Electrochemical Reduction of Carbon Dioxide and Carbon Monoxide into Methanol with Cobalt Phthalocyanine," *Angew. Chem. Int. Ed.* **2019**, *58*, 16172-16176. http://dx.doi.org/10.1002/anie.201909257

(27) Choi, J.; Wagner, P.; Gambhir, S.; Jalili, R.; MacFarlane, D. R.; Wallace, G. G.; Officer, D. L. "Steric Modification of a Cobalt Phthalocyanine/Graphene Catalyst To Give Enhanced and Stable Electrochemical CO2 Reduction to CO," *ACS Energy Lett.* **2019**, *4*, 666-672. http://dx.doi.org/10.1021/acsenergylett.8b02355

(28) Wang, M.; Torbensen, K.; Salvatore, D.; Ren, S.; Joulié, D.; Dumoulin, F.; Mendoza, D.; Lassalle-Kaiser, B.; Işci, U.; Berlinguette, C. P.; Robert, M. "CO_2 electrochemical catalytic reduction with a highly active cobalt phthalocyanine," *Nat. Commun.* **2019**, *10*, 3602. http://dx.doi.org/10.1038/s41467-019-11542-w

(29) Zhu, M.; Chen, J.; Guo, R.; Xu, J.; Fang, X.; Han, Y.-F. "Cobalt phthalocyanine coordinated to pyridine-functionalized carbon nanotubes with enhanced CO2 electroreduction," *Applied Catalysis B: Environmental* **2019**, *251*, 112-118. http://dx.doi.org/10.1016/j.apcatb.2019.03.047

(30) Wu, Y.; Jiang, Z.; Lu, X.; Liang, Y.; Wang, H. "Domino electroreduction of CO_2 to methanol on a molecular catalyst," *Nature* **2019**, *575*, 639-642. http://dx.doi.org/10.1038/s41586-019-1760-8

(31) Yang, Z.; Zhang, X.; Long, C.; Yan, S.; Shi, Y.; Han, J.; Zhang, J.; An, P.; Chang, L.; Tang, Z. "Covalently anchoring cobalt phthalocyanine on zeolitic imidazolate frameworks for efficient carbon dioxide electroreduction," *CrystEngComm* **2020**, *22*, 1619-1624. http://dx.doi.org/10.1039/C9CE01517E

(32) Li, T.-T.; Mei, Y.; Li, H.; Qian, J.; Wu, M.; Zheng, Y.-Q. "Highly Selective and Active Electrochemical Reduction of CO2 to CO on a Polymeric Co(II) Phthalocyanine@Graphitic Carbon Nitride Nanosheet–Carbon Nanotube Composite," *Inorg. Chem.* **2020**. http://dx.doi.org/10.1021/acs.inorgchem.0c01977

(33) Xia, Y.; Kashtanov, S.; Yu, P.; Chang, L.-Y.; Feng, K.; Zhong, J.; Guo, J.; Sun, X. "Identification of dual-active sites in cobalt phthalocyanine for electrochemical carbon dioxide reduction," *Nano Energy* **2020**, *67*, 104163. http://dx.doi.org/10.1016/j.nanoen.2019.104163

(34) Wang, X.; Cai, Z.-F.; Wang, Y.-Q.; Feng, Y.-C.; Yan, H.-J.; Wang, D.; Wan, L.-J. "In Situ Scanning Tunneling Microscopy of Cobalt-Phthalocyanine-Catalyzed CO2 Reduction Reaction," *Angew. Chem. Int. Ed.* **2020**, *59*, 16098-16103. http://dx.doi.org/10.1002/anie.202005242

(35) Wu, Y.; Hu, G.; Rooney, C. L.; Brudvig, G. W.; Wang, H. "Heterogeneous Nature of Electrocatalytic CO/CO2 Reduction by Cobalt Phthalocyanines," *ChemSusChem* **2020**, *n/a*. http://dx.doi.org/10.1002/cssc.202001396

(36) Huai, M.; Yin, Z.; Wei, F.; Wang, G.; Xiao, L.; Lu, J.; Zhuang, L. "Electrochemical CO_2 reduction on heterogeneous cobalt phthalocyanine catalysts with different carbon supports," *Chem. Phys. Lett.* **2020**, *754*, 137655. http://dx.doi.org/10.1016/j.cplett.2020.137655

(37) Zeng, J. S.; Corbin, N.; Williams, K.; Manthiram, K. "Kinetic Analysis on the Role of Bicarbonate in Carbon Dioxide Electroreduction at Immobilized Cobalt Phthalocyanine," *ACS Catal.* **2020**, *10*, 4326-4336. http://dx.doi.org/10.1021/acscatal.9b05272

(38) De Riccardis, A.; Lee, M.; Kazantsev, R. V.; Garza, A. J.; Zeng, G.; Larson, D. M.; Clark, E. L.; Lobaccaro, P.; Burroughs, P. W. W.; Bloise, E.; Ager, J. W.; Bell, A. T.; Head-Gordon, M.; Mele, G.; Toma, F. M. "Heterogenized Pyridine-Substituted Cobalt(II) Phthalocyanine Yields Reduction of CO2 by Tuning the Electron Affinity of the Co Center," *ACS Appl. Mater. Interfaces* **2020**, *12*, 5251-5258. http://dx.doi.org/10.1021/acsami.9b18924

(39) Han, N.; Wang, Y.; Ma, L.; Wen, J.; Li, J.; Zheng, H.; Nie, K.; Wang, X.; Zhao, F.; Li, Y.; Fan, J.; Zhong, J.; Wu, T.; Miller, D. J.; Lu, J.; Lee, S.-T.; Li, Y. "Supported Cobalt Polyphthalocyanine for High-Performance Electrocatalytic CO_2 Reduction," *Chem* **2017**, *3*, 652-664. http://dx.doi.org/10.1016/j.chempr.2017.08.002

(40) Lin, L.; Li, H.; Yan, C.; Li, H.; Si, R.; Li, M.; Xiao, J.; Wang, G.; Bao, X. "Synergistic Catalysis over Iron-Nitrogen Sites Anchored with Cobalt Phthalocyanine for Efficient CO2 Electroreduction," *Adv Mater* **2019**, *31*, e1903470. http://dx.doi.org/10.1002/adma.201903470

(41) Lin, L.; Liu, T.; Xiao, J.; Li, H.; Wei, P.; Gao, D.; Nan, B.; Si, R.; Wang, G.; Bao, X. "Enhancing CO2 Electroreduction to Methane with a Cobalt Phthalocyanine and Zinc-Nitrogen-Carbon Tandem Catalyst," *Angew Chem Int Ed Engl* **2020**, *59*, 22408-22413. http://dx.doi.org/10.1002/anie.202009191

(42) Zhang, H.; Min, S.; Wang, F.; Zhang, Z. "Immobilizing cobalt phthalocyanine into a porous carbonized wood membrane as a self-supported heterogenous electrode for selective and stable CO2 electroreduction in water," *Dalton Trans* **2020**, *49*, 15607-15611. http://dx.doi.org/10.1039/d0dt03304a

(43) Liu, Y.; Leung, K. Y.; Michaud, S. E.; Soucy, T. L.; McCrory, C. C. L. "Controlled Substrate Transport To Electrocatalyst Active Sites For Enhanced Selectivity In The Carbon Dioxide Reduction Reaction," *Comments Inorg. Chem.* **2019**, 1-28. http://dx.doi.org/10.1080/02603594.2019.1628025

(44) Canty, A. J.; Barron, P.; Healy, P. C. "1H and 199Hg NMR spectra of methylmercury(II) complexes. Effects of basicity and ortho substitution in pyridines(L) in complexes [MeHgL]NO3," *J. Organomet. Chem.* **1979**, *179*, 447-458. http://dx.doi.org/10.1016/S0022-328X(00)91861-8

(45) Canty, A. J.; Chaichit, N.; Gatehouse, B. M.; George, E. E.; Hayhurst, G. "Coordination chemistry of methylmercury(II). Synthesis, hydrogen-1 NMR, and crystallographic studies of cationic complexes of MeHg(II) with ambidentate and polydentate ligands containing pyridyl and N-substituted imidazolyl donors and involving unusual coordination geometries," *Inorg. Chem.* **1981**, *20*, 2414-2422. http://dx.doi.org/10.1021/ic50222a011

(46) Canty, A. J.; Lee, C. V. "Interaction of methylmercury(II) with N-substituted pyrazoles. .sigma.-Donor ability of pyridines, imidazoles, and pyrazoles," *Organometallics* **1982**, *1*, 1063-1066. http://dx.doi.org/10.1021/om00068a012

(47) Canty, A. J.; Lee, C. V. "Relative σ donor ability of pyridines, imidazoles, and pyrazoles," *Inorg. Chim. Acta* **1981**, *54*, L205-L206. http://dx.doi.org/10.1016/S0020-1693(00)95435-5

(48) Rabenstein, D. L. "The aqueous solution chemistry of methylmercury and its complexes," *Acc. Chem. Res.* **1978**, *11*, 100-107. http://dx.doi.org/10.1021/ar50123a004

(49) Nyokong, T. "Equilibrium and kinetic studies of the reaction between pyridine and cobalt(II) phthalocyanine in DMSO," *Polyhedron* **1995**, *14*, 2325-2329. http://dx.doi.org/http://dx.doi.org/10.1016/0277-5387(95)00090-F

(50) Liaudet, E.; Battaglini, F.; Calvo, E. J. "Electrochemical study of sulphonated ferrocenes as redox mediators in enzyme electrodes," *J. Electroanal. Chem.* **1990**, *293*, 55-68. http://dx.doi.org/10.1016/0022-0728(90)80052-8

(51) Oyama, N.; Anson, F. C. "Catalysis of electrode processes by multiply-charged metal complexes electrostatically bound to polyelectrolyte coatings on graphite electrodes, and the use of polymer-coated rotating disk electrodes in diagnosing kinetic and conduction mechanisms," *Anal. Chem.* **1980**, *52*, 1192-1198. http://dx.doi.org/10.1021/ac50058a009

(52) Leddy, J.; Bard, A. J. "Polymer films on electrodes: Part XII. Chronoamperometric and rotating disk electrode determination of the mechanism of mass transport through poly(vinyl ferrocene) films," *J. Electroanal. Chem.* **1983**, *153*, 223-242. http://dx.doi.org/10.1016/S0022-0728(83)80015-1

(53) Leddy, J.; Bard, A. J.; Maloy, J. T.; Savéant, J. M. "Kinetics of film-coated electrodes: Effect of a finite mass transfer rate of substrate across the film—solution interface at steady state," *J. Electroanal. Chem.* **1985**, *187*, 205-227. http://dx.doi.org/10.1016/0368-1874(85)85779-8

(54) Compton, R. G.; Laing, M. E.; Ledwith, A.; Abu-Abdoun, I. I. "Polymer-coated electrodes: cyclic voltammetry and chronoamperometry of non-ideal systems — the anodic oxidation of poly(4-vinyl-triphenylamine) films," *J. Appl. Electrochem.* **1988**, *18*, 431-440. http://dx.doi.org/10.1007/BF01093759

(55) Shao, Y.; Gan, Z.; Epifanovsky, E.; Gilbert, A. T. B.; Wormit, M.; Kussmann, J.; Lange, A. W.; Behn, A.; Deng, J.; Feng, X.; Ghosh, D.; Goldey, M.; Horn, P. R.; Jacobson, L. D.; Kaliman, I.; Khaliullin, R. Z.; Kuś, T.; Landau, A.; Liu, J.; Proynov, E. I.; Rhee, Y. M.; Richard, R. M.; Rohrdanz, M. A.; Steele, R. P.; Sundstrom, E. J.; Woodcock, H. L.; Zimmerman, P. M.; Zuev, D.; Albrecht, B.; Alguire, E.; Austin,

B.; Beran, G. J. O.; Bernard, Y. A.; Berquist, E.; Brandhorst, K.; Bravaya, K. B.; Brown, S. T.; Casanova, D.; Chang, C.-M.; Chen, Y.; Chien, S. H.; Closser, K. D.; Crittenden, D. L.; Diedenhofen, M.; DiStasio, R. A.; Do, H.; Dutoi, A. D.; Edgar, R. G.; Fatehi, S.; Fusti-Molnar, L.; Ghysels, A.; Golubeva-Zadorozhnaya, A.; Gomes, J.; Hanson-Heine, M. W. D.; Harbach, P. H. P.; Hauser, A. W.; Hohenstein, E. G.; Holden, Z. C.; Jagau, T.-C.; Ji, H.; Kaduk, B.; Khistyaev, K.; Kim, J.; Kim, J.; King, R. A.; Klunzinger, P.; Kosenkov, D.; Kowalczyk, T.; Krauter, C. M.; Lao, K. U.; Laurent, A. D.; Lawler, K. V.; Levchenko, S. V.; Lin, C. Y.; Liu, F.; Livshits, E.; Lochan, R. C.; Luenser, A.; Manohar, P.; Manzer, S. F.; Mao, S.-P.; Mardirossian, N.; Marenich, A. V.; Maurer, S. A.; Mayhall, N. J.; Neuscamman, E.; Oana, C. M.; Olivares-Amaya, R.; O'Neill, D. P.; Parkhill, J. A.; Perrine, T. M.; Peverati, R.; Prociuk, A.; Rehn, D. R.; Rosta, E.; Russ, N. J.; Sharada, S. M.; Sharma, S.; Small, D. W.; Sodt, A. "Advances in molecular quantum chemistry contained in the Q-Chem 4 program package," *Mol. Phys.* **2015**, *113*, 184-215. http://dx.doi.org/10.1080/00268976.2014.952696

(56) Chai, J.-D.; Head-Gordon, M. "Long-range corrected hybrid density functionals with damped atom–atom dispersion corrections," *Physical Chemistry Chemical Physics* **2008**, *10*, 6615-6620. http://dx.doi.org/10.1039/B810189B

(57) Marenich, A. V.; Olson, R. M.; Kelly, C. P.; Cramer, C. J.; Truhlar, D. G. "Self-Consistent Reaction Field Model for Aqueous and Nonaqueous Solutions Based on Accurate Polarized Partial Charges," *J. Chem. Theory Comput.* **2007**, *3*, 2011-2033. http://dx.doi.org/10.1021/ct7001418

(58) Khaliullin, R. Z.; Bell, A. T.; Head-Gordon, M. "Analysis of charge transfer effects in molecular complexes based on absolutely localized molecular orbitals," *J. Chem. Phys.* **2008**, *128*, 184112. http://dx.doi.org/10.1063/1.2912041

(59) Ramdhanie, B.; Zakharov, L. N.; Rheingold, A. L.; Goldberg, D. P. "Synthesis, Structures, and Properties of a Series of Four-, Five-, and Six-Coordinate Cobalt(III) Triazacorrole Complexes: The First

Examples of Transition Metal Corrolazines," *Inorg. Chem.* **2002**, *41*, 4105-4107. http://dx.doi.org/10.1021/ic020297x

(60) Zhang, Y.-L.; Ruan, W.-J.; Zhao, X.-J.; Wang, H.-G.; Zhu, Z.-A. "Synthesis and characterization of axial coordination cobalt(III) complexes containing chiral Salen ligands," *Polyhedron* **2003**, *22*, 1535-1545. http://dx.doi.org/10.1016/S0277-5387(03)00261-4

(61) Li, N.; Wang, Y.; Wu, C.; Lu, W.; Pei, K.; Chen, W. "Bioinspired catalytic generation of high-valent cobalt-oxo species by the axially coordinated CoPc on pyridine-functionalized MWCNTs for the elimination of organic contaminants," *Appl. Surf. Sci.* **2018**, *434*, 1112-1121. http://dx.doi.org/10.1016/j.apsusc.2017.11.048

Table of Contents Image